Ca-asp bound X-ray structure and inhibition of *Bacillus anthracis* dihydroorotase (DHOase)

Amy J. Rice, **Hao Lei**, **Bernard D. Santarsiero**, **Hyun Lee**[*], and **Michael E. Johnson**[*]

[1]Center for Biomolecular Sciences and Department of Medicinal Chemistry and Pharmacognosy, University of Illinois at Chicago, 900 S. Ashland, IL 60607, USA

Graphical abstract
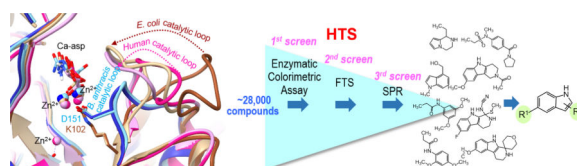
1. Introduction

The pyrimidine biosynthesis pathway is an attractive target for antibacterial drug design, as cells rely on nucleotide synthesis for survival and proliferation, and pyrimidines are essential building blocks of RNA and DNA. Mammals have a large, multifunctional dihydroorotate synthetase (CAD) enzyme for the first three steps of the *de novo* pyrimidine biosynthesis pathway, while prokaryotes use three separate monofunctional enzymes for each.[1, 2] Dihydroorotase (DHOase), the third enzyme in the *de novo* pathway, is responsible for the reversible cyclization of carbamyl-asparate (Ca-asp) to dihydroorotate (DHO) (Fig. 1A). Historically, DHOase was divided into two evolutionary classes, with very low sequence identity (< 30%) between classes. Class I DHOases are found in gram-positive bacteria, mold, and insects, while Class II DHOases are found in gram-negative bacteria and fungi. There are two distinct differences between these two classes of DHOases. First, the main differences are structural, with Class II being slightly smaller at ~38 kDa, and with a long flexible catalytic loop, compared to ~45 kDa Class I enzymes with either no or a very short corresponding loop. Second, DHOases contain four conserved histidines and one aspartate that coordinate the active site Zn^{2+} ions. Two active site Zn^{2+} ions in Class I are bridged by an aspartate, whereas a carboxylated lysine serves the same role in Class II. More recently, a third class has been suggested for human and *Porphyromonas gingivalis* DHOases because they have higher sequence similarity to Class I, but have a long catalytic loop and the active site Zn^{2+} ions are bridged by a carboxylated lysine, distinctive to Class II (Fig. 1B).[3]

[*]To whom correspondence should be addressed. Michael E. Johnson: (Phone) 312-996-9114, (Fax) 312-413-9303, mjohnson@uic.edu, Hyun Lee: (Phone) 312-413-9304, (Fax) 312-413-9303, danielhl@uic.edu.

So far, the Class II DHOase from *Escherichia coli* has been most extensively studied, producing many apo and complex structures. The structure revealed DHOase to be a homodimer zinc metalloenzyme that belongs to the 'amidohydrolase superfamily', a classification proposed for a group of functionally diverse metal-dependent hydrolase enzymes with a central $(\beta/\alpha)^8$ barrel fold in the catalytic domain.[4,5] The mechanism of DHOase was structurally determined as well, and is a cyclization reaction where the Ca-asp is stabilized by the active site Zn^{2+} and several active site residues (Asn44, Arg20, His254), while the carboxylate of Asp250 abstracts a proton from the amide nitrogen of Ca-asp, allowing for a nucleophilic attack (Fig. 1C).[2] The proposed chemical mechanism coincides with previously observed effects of pH on DHOase activity, where the forward enzymatic reaction is favored at lower pH, while the reverse reaction is favored at higher pH.[6,7]

Crystal structures of ligand-bound DHOase show that the catalytic loop extends toward the active site when Ca-asp is bound, whereas it is in an 'out' formation when DHO is the substrate.[8–10] The ligand and inhibitor complexes of *E. coli* DHOase and mutagenesis studies identified the importance of two threonine residues (T109, T110) on the flexible loop of Class II DHOase to stabilize the transition-state of Ca-asp, with T110 mutations resulting in decreased activity and T109 mutations demonstrating the essentiality of the hydrogen bond interaction from the hydroxyl group for converting Ca-asp to DHO (Fig. 1C).[8–12] However, Class I DHOase has no distinct loop, and there are no structures of substrate or inhibitor bound Class I enzymes available to date to elucidate the interactions that would replace the role of these important threonines.

Currently, no inhibitors for gram-positive bacterial DHOase have been identified. *Bacillus anthracis* is the Gram-positive etiologic agent of anthrax, and DHOase has been identified as critical for its survival in human serum.[13] Human anthrax infections can be developed through exposure via skin, ingestion of infected animals, inhalation of spores, or more recently, by injection.[14] Early diagnosis and treatment is critical, but can be difficult if the person is unaware of being exposed to the pathogen as the initial clinical presentation is consistent with flu-like symptoms.[15] Even with treatment, the mortality rates of gastrointestinal and inhalation anthrax are >40%.[16, 17] Current treatment is focused on post-exposure prophylaxis (PEP), using a combination of antibiotics and antitoxins. Unfortunately, the long term therapy recommended with antimicrobials, such as β-lactams, introduce the risk of developing resistance. Therefore, developing novel antibiotics against *B. anthracis* would increase treatment options and make anthrax bioterrorism attacks less feasible.

Here, we present the first crystal structure of substrate-bound *B. anthracis* DHOase, which provides further insight into the differences in the catalytic loop between Class I and Class II DHOase and the role it may play in inhibitor or substrate binding and recognition. We previously screened inhibitors of Class II DHOase and DHO analogs against *B. anthracis* DHOase, and observed little to no inhibition.[18] To identify potential inhibitors, we screened ~28,000 compounds and fragments against *B. anthracis* DHOase using a high throughput enzymatic colorimetric assay[18, 19] and a thermal shift binding assay[20–23], followed by an "orthogonal" surface plasmon resonance analysis.[24]

2. Results and discussion

2.1 Structure of substrate-bound DHOase from *B. anthracis*

Class II DHOase from *E. coli* has been extensively studied with many reported crystal structures of apo wild-type and mutants and complexes with substrates or inhibitors.[8–10, 12] However, only apo structures have been solved for the two Gram positive bacteria DHOases from *B. anthracis* and *Staphylococcus aureus*. Here, we report the first substrate-bound crystal structure of a bacterial Class I DHOase. (PDB: 4YIW) The Ca-asp bound *B. anthracis* DHOase structure was solved and deposited as a homodimer at 2.45 Å, with chains A and B in one asymmetric unit. The substrate, Ca-asp, was found in the active site of each monomer, and both substrates have relatively weak electron density due to low substrate occupancy (Fig. 2A). The data processing and structure refinement statistics are summarized in Table 1. The overall structure of *B. anthracis* DHOase in complex with the Ca-asp looks similar to the apo structure (PDB: 3MPG) with an overall RMSD of 0.359 Å, indicating that binding of the Ca-asp did not cause much structural change. An overlay of Ca-asp-bound *E. coli* DHOase (PDB:1XGE) and our *B. anthracis* DHOase complex structure reveal a nice overlap in the catalytic aspartic acid (D250 and D304 in Fig. 2B). Another aspartate (D151) of *B. anthracis* DHOase aligns well with the carboxylated lysine (K102) of *E. coli* DHOase, serving the same purpose of bridging two active site Zn^{2+} ions. These two Zn^{2+} ions hold the substrate Ca-asp in position along with the active site residues, Arg60, Asn93, and His308, which also overlap well, suggesting the substrate is stabilized by the same hydrogen bond interactions. However, a major structural difference between the Class I and Class II DHOase is the longer catalytic loop of the Class II counterparts (shown in brown color in Fig. 2C). In the case of *E. coli* DHOase, previous studies have shown that the hydrogen bond interaction between Ca-asp and the two threonines (T109 and T110) on the catalytic loop play a crucial role.[10] However, neither of the threonine residues is present in *B. anthracis* DHOase, so it has been previously hypothesized that the glycine (G152) in the shorter Class I loop may serve this function.[3] According to our complex structure, this could be the case since the peptide backbone hydrogen of glycine is located at a distance of 3.75 Å from Ca-asp, which is within weak H-bond interaction range. (shown in blue dotted line in Fig. 2C). Flexible catalytic loops from the three DHOase classes are aligned for comparison (Fig. 2D and Fig. 2E). In the case of both Class II and III, long catalytic loops showed a distinct shift (dotted arrows) in the substrate-bound structures, indicating the regulatory role of the loops. On the other hand, the corresponding loop of *B. anthracis* DHOase (Class I) is very short and remained in the same location in the presence and absence of the substrate Ca-asp, and whether this loop plays the same stabilizing role or not is yet to be determined.

2.2 Mutagenesis Studies

Based on our substrate bound crystal structure, three active site residues (Arg63, Asn93, and Asp304) appear to stabilize the substrate and Zn^{2+} ion, indicating that these three residues could affect enzyme activity of *B. anthracis* DHOase. To further elucidate substrate-enzyme interactions, the three residues were sequentially mutated to an alanine. The affinities (K_M) of wild-type *B. anthracis* DHOase for Ca-asp and DHO are essentially identical, at 112 ± 24 μM and 114 ± 15 μM, respectively (Table 2). In contrast, the affinities of *E. coli* DHOase for Ca-asp and DHO differ significantly, with K_M values of 1700 μM and 80 μM, respectively.[2]

The catalytic activities of *B. anthracis* DHOase and *E. coli* DHOase also differ. For instance, the *E. coli* DHOase k_{cat} values for Ca-asp and DHO are 160 ± 8 s^{-1} and 100 ± 1.6 s^{-1}, respectively, compared to 2.1 ± 0.1 s^{-1} and 1.9 ± 0.1 s^{-1} for *B. anthracis* DHOase. This finding is similar to the catalytic kinetics of *S. aureus* DHOase, another active Class I DHOase.[25] Interestingly, the catalytic efficiency (k_{cat}/K_M) of *B. anthracis* DHOase with Ca-asp as the substrate is similar to that of *E. coli* DHOase when Thr110 is mutated to Serine, and the essential Thr109 is maintained. The serine could still make the hydrogen bond interaction between the loop and Ca-asp, but this mutation caused a 6-fold decrease in k_{cat}/K_M compared to the wild-type, making its activity comparable to that of *B. anthracis* and *S. aureus* DHOases. Previously, it has been hypothesized that either the glycine in the shorter loop of Class I DHOase or the ATCase domain plays the critical role of the threonines in Class I DHOase, explaining why some Class I DHOase are active, while others, such as *A. aeolicus* DHOase is inactive unless it associates with the ATCase domain. The comparison of our kinetic parameters suggests that although the peptide backbone of glycine in Class I DHOase may contribute H-bond interactions for enzyme activity, an association with the ATCase domain may increase the enzyme activity. Despite the ~6-fold difference in k_{cat}/K_M values, the crystal structures show that Ca-asp binds in a similar manner in both classes of DHOase and has the same physicochemical interactions with the active site residues.

The *E. coli* DHOase Asp250 stabilizes a Zn^{2+} ion and initiates the enzyme reaction, and this aspartic acid residue is required for catalytic activity. This is also the case for Class I *B. anthracis* DHOase, as mutagenesis of D304 to alanine completely abolished activity in *B. anthracis* DHOase, with minimal recovery of activity after supplementing with zinc sulfate up to 2.5 mM. The R63A mutant also showed no enzyme activity with either DHO or Ca-asp. This is because Arg63 stabilizes the exocyclic carboxylic acid of both the substrate and product in the active site. On the other hand, Asn93 has an electrostatic interaction with the carboxylic group of Ca-asp, which undergoes nucleophilic attack by the amide nitrogen to form DHO. The N93A mutant has minor activity, even with almost 10-fold higher concentrations of Ca-asp compared to wild-type DHOase, most likely due to the inability to stabilize Ca-asp in the active site. When DHO is the substrate, no enzyme activity is observed, presumably because DHO lacks the carboxylic terminal to interact with Asn93 (Table 2).

2.3 High-throughput Screening and hit validation

Previously, inhibitors of *E. coli* and *P. falciparum* DHOase, such as 5-fluoroorotate (FOA), 5-aminoorotate (AOA), and three analogs of DHO showed no inhibition of *B. anthracis* DHOase.[18] Therefore, to identify inhibitors for *B. anthracis* DHOase, a high-throughput screen (HTS) of 3,352 fragments from the Chembridge fragment and Zenobia fragment libraries were performed using a colorimetric enzymatic assay. A second thermal shift binding assay was performed to identify those that bind to the target enzyme. The enzymatic colorimetric assay uses a DAMO-TSC color mix to detect the ureido moiety of Ca-asp, as previously described.[18] Compounds that inhibit DHOase should prevent the reverse cyclization process from DHO to Ca-asp. Therefore, absence or lowered concentrations of Ca-asp will exhibit little to no color change. For our studies, any fragment that showed <

50% of color development (red square in Fig. 3A) compared to the control suggested enzyme activity inhibition and were considered to be initial hits. HTS using this method resulted in 142 hits. The thermal shift binding assay uses a fluorescence dye to monitor unfolding and exposure of hydrophobic regions of an enzyme while gradually increasing the temperature.[26] If a fragment binds to DHOase, it should stabilize the enzyme, resulting in a shift in melting temperature (T_m) to a higher temperature (Fig. 3C). Fragments that showed > 2 °C shift in temperature were identified as hits (Fig. 3B). This second method of HTS resulted in 160 hits, with 10 fragments overlapping with the enzymatic screen. One of the disadvantages of the fluorescence thermal shift assay is that fragments which saturate the target may not show any temperature shift by displaying a broad fluorescence curve. For that reason, we did not want to disregard any promising hits from our enzymatic assay. After testing the enzymatic hits for compound interference on color development, we selected 14 fragments to perform a secondary confirmation assay. Surface plasmon resonance (SPR) was used to eliminate non-specific binders and to determine the binding affinity (dissociation equilibrium constant, K_D). Promiscuous binders were identified as those that did not show a trend toward a saturable curve (Fig. S5). Sensorgrams of compound **4** are shown at eight different concentrations in Fig. 3D as an example, and the determined K_D values of 8 final fragment hits varied between 67 μM and 334 μM (Fig. 4).

2.4 Identification of a lead compound and Structure-Activity Relationship (SAR)

To determine if the inhibitors bind to the active site, the K_D was determined for each compound in the absence and presence of substrate Ca-asp (Fig. 4). If the compounds bind to the active site, the expectation is that the compound K_D should be affected by the presence of high concentration of substrate. Overall, the binding affinity did not change in the presence of 1 mM Ca-asp, suggesting the hits may not be competitive inhibitors, with the exception of compound 7 (Fig. S7). These results suggest that the compounds may bind to an allosteric site, or possibly in the active site but not in a position to compete with substrate. Our crystal structure shows an open active site with a large chemical space which could accommodate two smaller fragments, such as our hit compounds and the natural substrate. This possibility could be observed when comparing compounds 3 and 4. Compounds **3** and **4** are similar in structure with similar binding affinities of 157 ± 2 μM and 170 ± 4 μM, respectively. However, with 1 mM Ca-asp, the K_D of compound **3** nearly doubled, to 281 ± 19 μM, indicating that Ca-asp and **3** may be competing at least in part for the active site, whereas that of compound **4** remained the same. Previously, it has been shown that DHOase is highly specific for its substrate, and the substitution positions played a critical role, in that 5-substituted analogs of the substrate were more effective inhibitors and more competitive for the position in the active site that is normally occupied by either DHO or Ca-asp.[27] Additionally, this may explain why compound **3** exhibited competition with the substrate, while compound **4** did not. Compounds **6**–**8** have a similar and much more rigid 3-ring scaffold, with compound **7** having the highest affinity for DHOase with a K_D value of 67 ± 7 μM. Interestingly, in the presence of substrate, the binding affinity weakened significantly enough that K_D was unable to be determined, confirming that **7** is a competitive inhibitor.

A few commercially available fragment analogs of compounds **6** and **7** were obtained and tested by SPR, and a preliminary Structure-Activity-Relationships (SAR) is summarized in

Table 3. When the tetrahydro-*2H*-pyran ring of compound **6** was removed from R^2 position, the K_D increased ~1.5-fold, going from 380 μM to 588 μM and was not affected by the addition of substrate. When the methoxy group of **6a** in the R^1 position was replaced by a methyl group (**6b**), the compound interaction with DHOase was completely abolished. Similarly, when the methoxy group in the R^1 was retained, but the tetrahydropyridine of R^2 was removed (**6c**), the compound also showed no interaction with DHOase, indicating the interactions of the methoxy group and pyridine ring are necessary for active site binding. When the R^1 position was kept as the same methoxy group and the pyran ring in R^1 position was substituted by thiomethyl and cyanamide (**7a**), the binding affinity increased 18-fold from 380 μM to 21 μM, most likely due to the interaction between cyanamide and the Zn ions in the active site. When the methoxy group replaced the fluorine (**7**) in R^1 position and kept R^2 position same, the affinity decreased slightly to 84 μM. When the tetrahydropyridine ring was tethered with acetyl on the nitrogen (**8**) in the R^2 position, interaction became weaker. These results together suggest that fluorine is the most favored, and methoxy is tolerated in the R^1 position. A tetrahydropyridine in R^2 is required, and being tethered with thiomethyl and cyanamide is the most favored, while tetrahydropyridine alone, fused with pyran, or tethered with acetyl on the nitrogen is tolerated (Fig. 5). Based on this preliminary Structure-Activity Relationship (SAR) map, our lead compound, **7**, can be further optimized through synthesis.

3. Conclusions

We were able to solve the crystal structure of *B. anthracis* DHOase with Ca-asp in the active site (PDB: 4YIW). The structure confirms that the key interactions between the substrate and active site residues are similar between Class I and Class II DHOase enzymes, except for the lack of substrate stabilization by the catalytic loop in Class I DHOase. The crystal structure of *E. coli* (PDB:1XGE) shows two threonine residues that stabilize the substrate, which may also play a role in stabilizing small inhibitors. In contrast, the shorter loop in *B. anthracis* DHOase interaction with the substrate is minimal, and our structure confirms the previously hypothesized role of glycine as the hydrogen bond contributor. To further understand the importance of Ca-asp stabilization by hydrogen bonding, the enzyme kinetics will be compared to G152S and G152T in ongoing studies. The lack of loop stabilization may be one of the reasons why inhibitors of Class II DHOase have not been effective in *B. anthracis* DHOase. In order to identify potential inhibitors, we performed high-throughput screening of *B. anthracis* DHOase against several libraries using an enzymatic assay and an orthogonal binding assay. The binding affinity constants for eight inhibitors were determined by SPR, as well as by competition analysis with Ca-asp to determine if the inhibitors bound in the active site. The few hit compounds share a similar scaffold, and analogs were selected for further analysis based on binding affinities, with a preliminary SAR map. Our results provide more insight into the dihydroorotase family and identified several compounds that can be further optimized as potential antimicrobials against *B. anthracis*.

4. Experimental section

4.1 Preparation and purification of DHOase

The DHOase gene from *Bacillus anthracis* (Sterne strain) was cloned into a pET15b vector (Invitrogen) and purified as previously described.[18, 28] In brief, the recombinant plasmid was inserted into BL21(DE3) Gold cells (Invitrogen) and grown in Terrific Broth (TB) media (Fisher Scientific) at 37° C while shaking at 220 rpm until the OD_{600} reached 0.6, when it was induced with 1 mM isopropyl B-D-1-thiogalactopyranoside (IPTG) (Sigma) and incubated for an additional 4 hours before harvesting. The cell pellet was resuspended in 50 mM Tris, pH 8.0, 500 mM NaCl, 20 mM imidazole, and 5 mM β-mercaptoethanol (β-MCE), 1 mg/mL lysozyme, 0.01% Triton X-100, and 0.025 mg/mL DNase I, and lysed by sonication. A HisTrap HP column (GE Healthcare) was used to purify the histidine-tagged protein using a stepwise gradient of elution buffer (50 mM Tris, pH 8.0, 500 mM NaCl, 500 mM imidazole, and 5 mM β-MCE) with either an AKTA purifier or AKTAxpress FPLC system. The eluted protein was dialyzed in 50 mM Tris, pH 7.5, and 100 mM NaCl overnight to remove imidazole. The histidine tag was removed by incubating the dialyzed protein with 1.5 units of thrombin per mg protein at room temperature for 1 hour, followed by 45 minutes at 37 °C. The digested protein was reloaded onto a HisTrap HP column stacked with a HiTrap Benzamidine column that was equilibrated with 50 mM Tris, pH 8.0, 500 mM NaCl, and 5 mM β-MCE. The histidine-tag cleaved DHOase was collected in the flow-through and loaded onto a HiLoad 16/60 Superdex 75 PG gel filtration column that was equilibrated with 25 mM Tris, pH 7.5 and 100 mM NaCl. Protein samples were analyzed by SDS-PAGE and final purity was above 90%.

4.2 Site-directed mutagenesis

R63A, N93A, and D304A mutations on DHOase were generated by site-directed mutagenesis PCR using the NEB Q5 mutagenesis Kit and wild-type pET15b plasmid containing *B. anthracis* DHOase as a template. The primers used are as follows: R63A, 5'-GGATTAGTAGATGTACACGTACACCT GCAGAACCAGGTGGTGAACATAAAG-3'; N93A, 5'-CACTACAATTTGCGCAATGCCAGCAACACGCCCAGTACCAG-3'; D304A, 5'-GGAACAATCGATATGATCGCAACTGCACATGCACCGCATACAGC-3'. The PCR reaction contained 0.3 μM each of forward and reverse primers, 0.5 μL template, 12.5 μL Q5 Hot Start High-Fidelity 2X Mix, and sterile water adjusted to 50 μL total volume for each forward and reverse reaction. The PCR product was incubated with the provided Kinase-Ligase-DpnI enzyme mix for 30 minutes at room temperature. The final PCR product was transformed into DH5α cells via heat shock for 30 seconds at 42° C and plated onto ampicillin treated plates (ampicillin 100 μg/mL). Transformants with the correct mutation were used to extract the plasmid and retransform into a protein expression cell line, BL21(DE3) Gold cells, via heat shock at 42° C for 30 seconds. Each mutant was expressed and purified by the same way as the wild-type DHOase.

4.3 Enzyme kinetics determination

The Michaelis-Menten constant (K_M) was determined as described previously.[18, 25] In brief, the K_m values were determined by monitoring the UV absorbance at 230 nm. The reverse reaction of 100 nM final concentration wild-type DHOase or its mutants (R63A, N93A, or

D304A-DHOase) were performed in 50 mM Tris, pH 8.3 with concentrations of substrate DHO ranging from 0 – 500 μM at 2-fold serial dilution in a 96-well UV plate (Corning). The forward reaction was performed in the same manner, but with a different assay buffer consisting of 50 mM MES, pH 5.8 at 100 nM final concentration wild-type DHOase or its mutants. The substrate Ca-asp concentrations for wild-type and two mutants (R63A and D304A) DHOase reaction ranged from 0 – 650 μM, while a much higher concentration range (0 – 5 mM) was used for N93A-DHOase. The enzyme reaction was continuously monitored using a SPECTRAmax Plus (Molecular Devices). The K_M value and maximum activity (V_{max}) were calculated using Sigmaplot 11.0 to fit the data to the hyperbolic equation (1), where y is the initial velocity and x is the concentration of the substrate.

4.4 Crystallization of substrate-bound BaDHOase

The pooled histidine-tag cleaved wild-type DHOase was concentrated to 10 mg/mL. It was then incubated with 1.5 mM of either DHO or Ca-asp overnight on ice. DHOase was crystallized using hanging-drop vapor diffusion with the crystallization condition of 0.1 M Bis-Tris, pH 5.5, 0.2 M NaCl, and 20% PEG 3350. The crystals diffracted at λ= 0.979800 Å at 100K using a MARMOSAIC CCD 300 mm detector at an oscillation angle of 1.0° for 360 frames at the Advanced Photon Source LS-cat beamline, station 21-ID-D at the Argonne National Laboratory. The data was indexed, integrated, and scaled by XDS.[29] The molecular replacement was completed using Phaser[30] in CCP4 and the structural refinement was completed with Refmac5.5[31] and Coot[32].

4.5 Primary high-throughput screening

High-throughput screening of 3,352 fragments from the Chembridge fragment and Zenobia fragment libraries were performed using the Tecan Freedom EVO 200 liquid handling robot and the DAMO-TSC assay which has previously been optimized for this target.[18] All assays were done in duplicate in transparent 384-well plates (Grenier). 30 μL of 133 nM his-tagged DHOase in HTS buffer (50 mM Tris, pH 8.3, 0.01% Triton X-100, 0.1 mg/mL BSA, 4 mM TCEP) was dispensed to plates, and final concentrations of 400 μM of each fragment or 25 μM of each compound was added and incubated for 10 minutes at room temperature. Then 10 μL of 320 μM substrate DHO in the same assay buffer was added prior to incubation for another 30 minutes after 30 seconds of shaking. To quench the reaction, 64 μL of DAMO-TSC acid color mix was added. The assay plates were sealed and incubated in the dark for 16 hours at room temperature prior to measuring the absorbance at 540 nm. Each plate contained 32 positive and 32 negative controls.

4.6 Fluorescence thermal shift assay

A fluorescence thermal shift (FTS) binding assay was performed on 3,352 fragments. FTS assay plates were prepared by the Tecan Freedom EVO 200 liquid handling robot, and melting curves were monitored using a Viia7 Real-Time PCR (Applied Biosystems). 5 μL of histidine-tagged DHOase (5 μM final concentration) in FTS buffer consisting of 50 mM MES, pH 6.5, 0.01% CHAPS, 150 mM NaCl, and 2 mM TCEP was dispensed in white 384-well PCR plates (BioRad). 0.1 μL of each fragment (400 μM final concentration) was added to the plate using a 384-pin stainless steel pin tool (V&P Scientific) with a 100-nL capillary capacity and incubated for 10 minutes at room temperature. Then 5 μL of 10X SYPRO

Orange dye, diluted from 5000X stock, was added prior to shaking for 30 seconds. The assay plates were gradually heated from 25 °C to 95 °C at 0.07 °C/min while the fluorescence intensity was continuously measured at excitation/emission 470/623 nm. A Protein Thermal Shift™ Software (Applied Biosystems) was used to calculate the T^m shifts, and any fragments with $T^m > 2°$ C were identified as positive hits.

4.7 Hit validation with surface plasmon resonance

Purified histidine-tag cleaved DHOase was buffer exchanged to PBS-P (10 mM phosphate, pH 7.4, 2.7 mM KCl, 137 mM NaCl, and 0.05% surfactant P-20). Surface Plasmon Resonance was performed at 25 °C using a Biacore T200 instrument and a CM5 sensor chip. The flow channels were activated by a 1-ethyl-3-(3-dimethylaminopropyl) carbodiimide hydrocholoride (EDC)/N-hydroxy succinimide (NHS) mixture. DHOase was diluted in 10 mM sodium acetate (pH 4.5) and immobilized to flow channels 2, 3, and 4 at levels of 12,974 RU, 9,853 RU, and 12,150 RU, respectively. Flow channel 1 was blocked by ethanolamine (pH 8.5) as a control. Compound solutions at increasing concentrations (0–200 μM at 2-fold dilutions) in binding buffer were applied to all four channels at a 10 μL/min flow rate. The SPR binding buffer was PBS-P, 2% DMSO and 0.5 mM TCEP. 1 mM Ca-asp was added to the binding buffer for competition SPR. The sensorgrams were analyzed using Biaevaluation software 2.0.3. All data was reference with the blank channel response unit signal prior to the fitting. The response unit difference at each concentration was measured during the binding equilibrium phase and K_D values were determined using the steady-state affinity fitting equation embedded in the Biaevaluation software.

Supplementary Material

Refer to Web version on PubMed Central for supplementary material.

Acknowledgments

References

1. Evans DR, Guy HI. Mammalian pyrimidine biosynthesis: fresh insights into an ancient pathway. J Biol Chem. 2004; 279:33035–33038. [PubMed: 15096496]

2. Porter TN, Li Y, Raushel FM. Mechanism of the dihydroorotase reaction. Biochemistry. 2004; 43:16285–16292. [PubMed: 15610022]

3. Grande-García A, Lallous N, Díaz-Tejada C, Ramón-Maiques S. Structure, functional characterization, and evolution of the dihydroorotase domain of human CAD. Structure. 2014; 22:185–198. [PubMed: 24332717]

4. Holm L, Sander C. An evolutionary treasure: unification of a broad set of amidohydrolases related to urease. Proteins. 1997; 28:72–82. [PubMed: 9144792]

5. Liu, A.; Huo, L. Amidohydrolase Superfamily. eLS, John Wiley & Sons, Ltd; 2001.

6. Sander EG, Heeb MJ. Purification and properties of dihydroorotase from Escherichia coli B. Biochim Biophys Acta. 1971; 227:442–452. [PubMed: 4994515]

7. Wang CC, Tsau HW, Chen WT, Huang CY. Identification and characterization of a putative dihydroorotase, KPN01074, from Klebsiella pneumoniae. Protein J. 2010; 29:445–452. [PubMed: 20676924]

8. Lee M, Chan CW, Mitchell Guss J, Christopherson RI, Maher MJ. Dihydroorotase from Escherichia coli: loop movement and cooperativity between subunits. J Mol Biol. 2005; 348:523–533. [PubMed: 15826651]

9. Lee M, Chan CW, Graham SC, Christopherson RI, Guss JM, Maher MJ. Structures of ligand-free and inhibitor complexes of dihydroorotase from Escherichia coli: implications for loop movement in inhibitor design. J Mol Biol. 2007; 370:812–825. [PubMed: 17550785]

10. Lee M, Maher MJ, Christopherson RI, Guss JM. Kinetic and structural analysis of mutant Escherichia coli dihydroorotases: a flexible loop stabilizes the transition state. Biochemistry. 2007; 46:10538–10550. [PubMed: 17711307]

11. Lee M, Maher MJ, Guss JM. Structure of the T109S mutant of Escherichia coli dihydroorotase complexed with the inhibitor 5-fluoroorotate: catalytic activity is reflected by the crystal form. Acta Crystallogr Sect F Struct Biol Cryst Commun. 2007; 63:154–161.

12. Thoden JB, Phillips GN Jr, Neal TM, Raushel FM, Holden HM. Molecular structure of dihydroorotase: a paradigm for catalysis through the use of a binuclear metal center. Biochemistry. 2001; 40:6989–6997. [PubMed: 11401542]

13. Samant S, Lee H, Ghassemi M, Chen J, Cook JL, Mankin AS, Neyfakh AA. Nucleotide biosynthesis is critical for growth of bacteria in human blood. PLoS Pathog. 2008; 4:e37. [PubMed: 18282099]

14. Berger T, Kassirer M, Aran AA. Injectional anthrax - new presentation of an old disease. Euro Surveill. 2014; 19

15. Sweeney DA, Hicks CW, Cui X, Li Y, Eichacker PQ. Anthrax infection. Am J Respir Crit Care Med. 2011; 184:1333–1341. [PubMed: 21852539]

16. W.M. Hendricks KA, Shadomy SV, Bradley JS, Morrow MG, Pavia AT, et al. Centers for Disease Control and Prevention expert panel meetings on prevention and treatment of anthrax in adults. Emerg Infect Dis [Internet]. 2014

17. Owen JL, Yang T, Mohamadzadeh M. New insights into gastrointestinal anthrax infection. Trends Mol Med. 2015; 21:154–163. [PubMed: 25577136]

18. Rice AJ, Truong L, Johnson ME, Lee H. A colorimetric assay optimization for high-throughput screening of dihydroorotase by detecting ureido groups. Anal Biochem. 2013; 441:87–94. [PubMed: 23769705]

19. Knipp M, Vasak M. A colorimetric 96-well microtiter plate assay for the determination of enzymatically formed citrulline. Analytical Biochemistry. 2000; 286:257–264. [PubMed: 11067748]

20. Sorrell FJ, Greenwood GK, Birchall K, Chen B. Development of a differential scanning fluorimetry based high throughput screening assay for the discovery of affinity binders against an anthrax protein. J Pharm Biomed Anal. 2010; 52:802–808. [PubMed: 20376913]

21. Lo MC, Aulabaugh A, Jin G, Cowling R, Bard J, Malamas M, Ellestad G. Evaluation of fluorescence-based thermal shift assays for hit identification in drug discovery. Anal Biochem. 2004; 332:153–159. [PubMed: 15301960]

22. Layton CJ, Hellinga HW. Thermodynamic analysis of ligand-induced changes in protein thermal unfolding applied to high-throughput determination of ligand affinities with extrinsic fluorescent dyes. Biochemistry. 2010; 49:10831–10841. [PubMed: 21050007]

23. Pantoliano MW, Petrella EC, Kwasnoski JD, Lobanov VS, Myslik J, Graf E, Carver T, Asel E, Springer BA, Lane P, Salemme FR. High-density miniaturized thermal shift assays as a general strategy for drug discovery. J Biomol Screen. 2001; 6:429–440. [PubMed: 11788061]

24. Karlsson R. Real-time competitive kinetic analysis of interactions between low-molecular-weight ligands in solution and surface-immobilized receptors. Anal Biochem. 1994; 221:142–151. [PubMed: 7985785]

25. Truong L, Hevener KE, Rice AJ, Patel K, Johnson ME, Lee H. High-level expression, purification, and characterization of Staphylococcus aureus dihydroorotase (PyrC) as a cleavable His-SUMO fusion. Protein Expr Purif. 2013; 88:98–106. [PubMed: 23246866]

26. Andreotti G, Monticelli M, Cubellis MV. Looking for protein stabilizing drugs with thermal shift assay. Drug Test Anal. 2015

27. Christopherson RI, Jones ME. The effects of pH and inhibitors upon the catalytic activity of the dihydroorotase of multienzymatic protein pyr1–3 from mouse Ehrlich ascites carcinoma. J Biol Chem. 1980; 255:3358–3370. [PubMed: 6102565]

28. Mehboob S, Mulhearn DC, Truong K, Johnson ME, Santarsiero BD. Structure of dihydroorotase from Bacillus anthracis at 2.6 Å resolution. Acta Crystallogr Sect F Struct Biol Cryst Commun. 2010; 66:1432–1435.

29. Kabsch W. XDS. Acta Crystallogr D Biol Crystallogr. 2010; 66:125–132. [PubMed: 20124692]

30. McCoy AJ, Grosse-Kunstleve RW, Adams PD, Winn MD, Storoni LC, Read RJ. Phaser crystallographic software. J Appl Crystallogr. 2007; 40:658–674. [PubMed: 19461840]

31. Vagin AA, Steiner RA, Lebedev AA, Potterton L, McNicholas S, Long F, Murshudov GN. REFMAC5 dictionary: organization of prior chemical knowledge and guidelines for its use. Acta Crystallogr D Biol Crystallogr. 2004; 60:2184–2195. [PubMed: 15572771]

32. Emsley P, Lohkamp B, Scott WG, Cowtan K. Features and development of Coot. Acta Crystallogr D Biol Crystallogr. 2010; 66:486–501. [PubMed: 20383002]
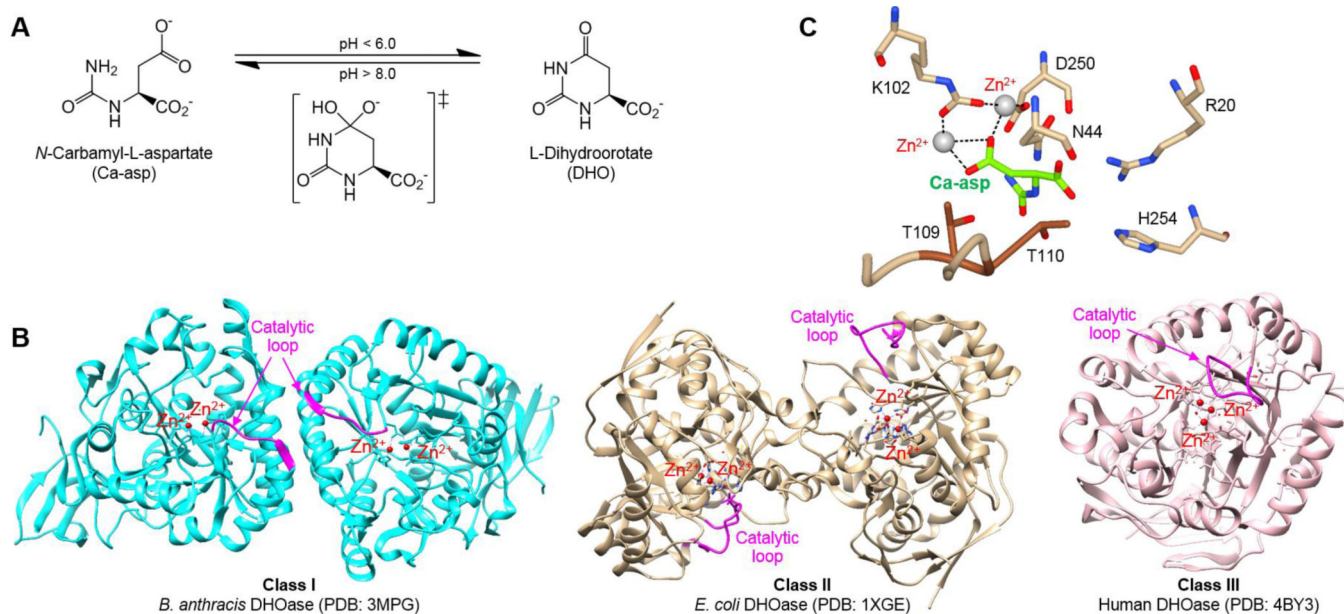
Figure 1. The mechanism of DHOase

(**A**) The enzyme catalyzes the reversible cyclization of Ca-asp to DHO. (**B**) Ca-asp is stabilized by the Zn^{2+} ions coordinated by a carboxylated K102, while D250 abstracts the proton from the amide nitrogen of Ca-asp. (PDB: 1XGE). The exocyclic carboxyl group of Ca-asp is stabilized by N44, R20, and H254, in addition to the T109 and T110 from the 'in' formation of the catalytic loop. (**C**) Comparison of the three classes of DHOase with the catalytic loop highlighted in pink.
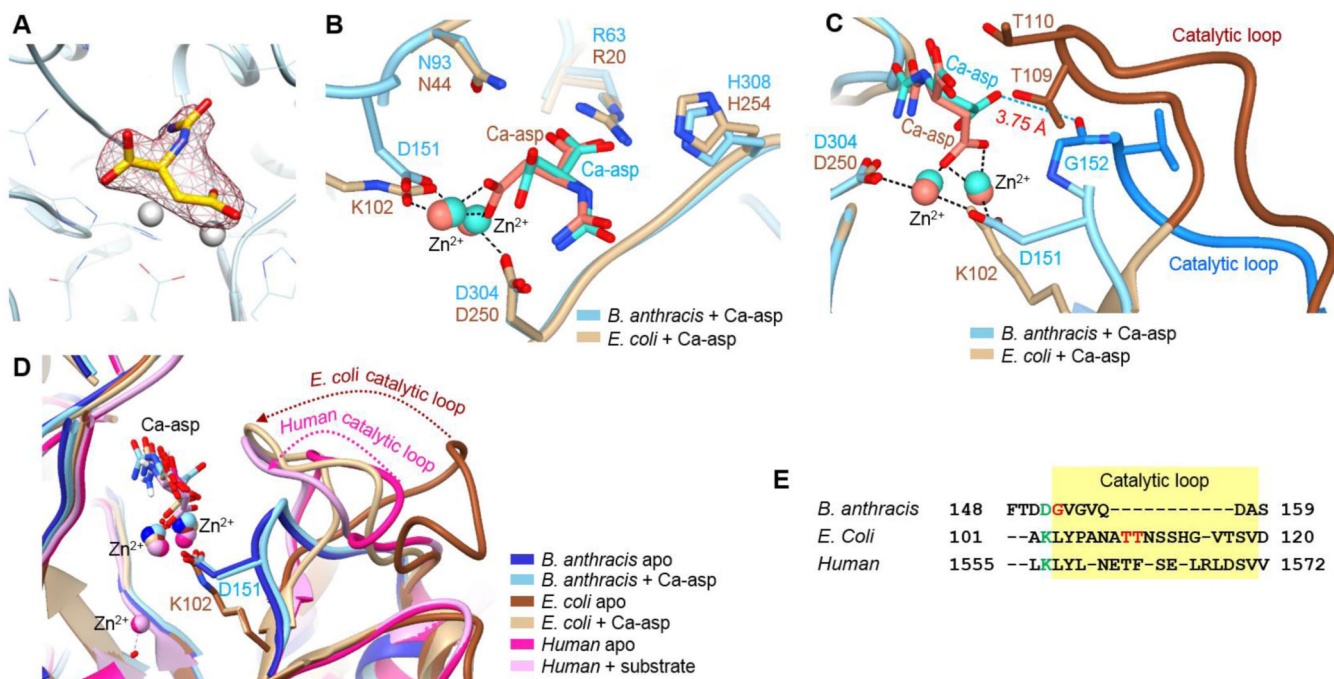
Figure 2. Comparison of Class I and Class II DHOase

(**A**) Electron density of Ca-asp in the active site. The ligand density is countered at $2F_o - F_c$ = 0.51 rmsd. (**B**) Overlay of substrate bound *B. anthracis* DHOase (PDB:4YIW, cyan) and *E. coli* DHOase (PDB:1XGE, tan). (**C**) Catalytic loop of *E. coli* DHOase (PDB:1XGE) highlighted in blue, and H-bond interaction of substrate with the peptide backbone of glycine in *B. anthracis* DHOase. (PDB:4YIW). (**D**) Overlay of the catalytic loop. (*B. anthracis* apo PDB:3MPG; *B. anthracis* + Ca-asp PDB:4YIW; *E. coli* apo PDB:2EG6; *E. coli* + Ca-asp PDB:1XGE; human apo PDB:4BYE; human + Ca-asp PDB:4C6I). (**E**) Sequence alignment of catalytic loop highlighted in yellow.
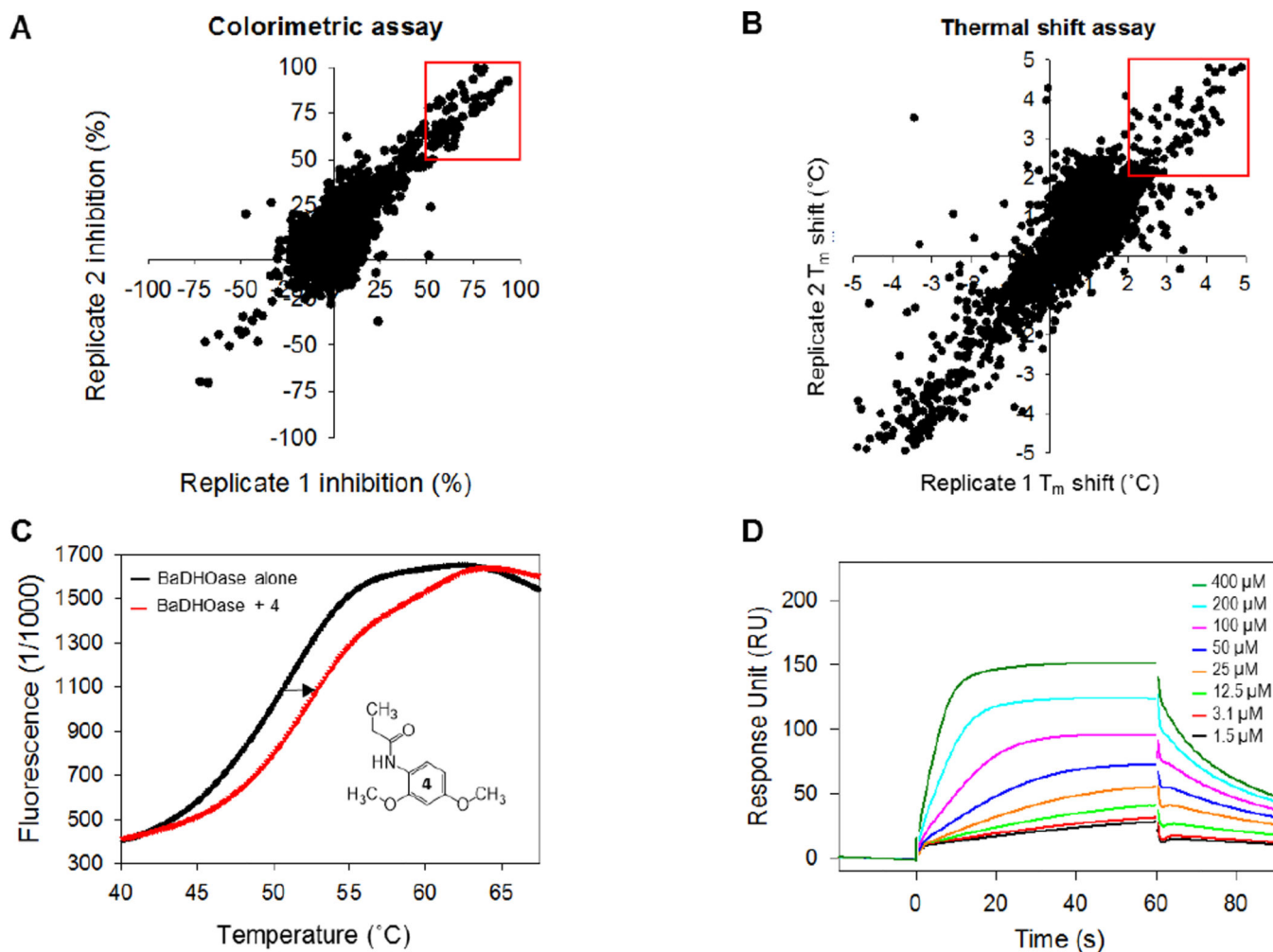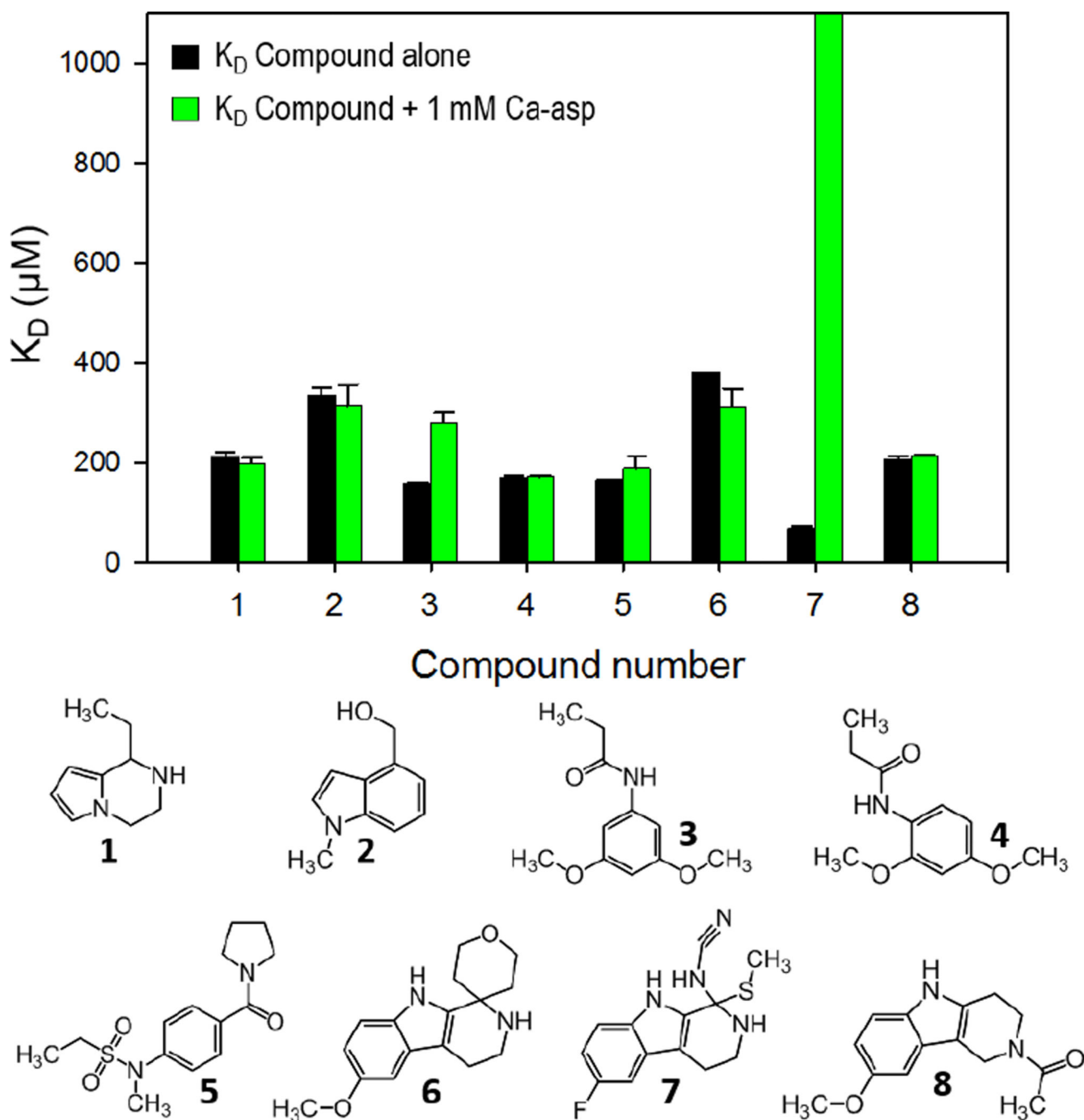
Figure 3. High-throughput screening (HTS) of DHOase
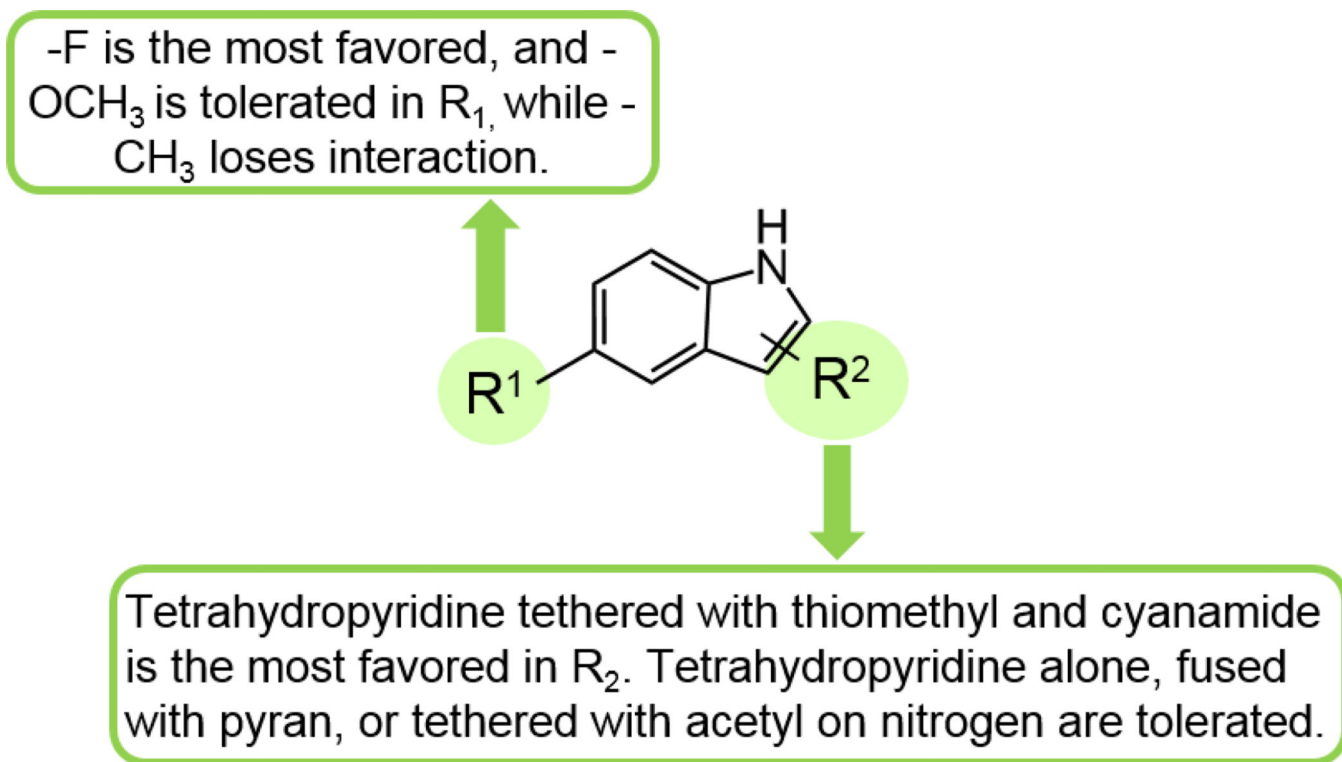
(**A**) Replicate plot of colorimetric enzymatic assay with fragments showing >50% inhibition in red. (**B**) Replicate plot of thermal shift binding assay with fragments showing >2 °C shift in red. (**C**) Melting curve of DHOase without substrate (black) and DHOase with Compound **4** (red). Compound **4** shows a shift in melting temperature (T_m) as indicated by the arrow. (**D**) Sensorgram of Compound **4** at increasing concentrations.

Figure 4. High-throughput screening hits

Bar graphs of the dissociation equilibrium constants (K_D) of 8 initial hit compounds determined by Surface Plasmon Resonance (SPR). K_D values were compared in the presence (green) and in the absence (black) of the substrate Ca-asp as a competitor. Bars that reached the top of the graph represent K_D values of over 1000 μM (no binding).

-F is the most favored, and -OCH$_3$ is tolerated in R$_1$, while -CH$_3$ loses interaction.

Tetrahydropyridine tethered with thiomethyl and cyanamide is the most favored in R$_2$. Tetrahydropyridine alone, fused with pyran, or tethered with acetyl on nitrogen are tolerated.

Figure 5. Preliminary Structure-Activity Relationship (SAR) map of HTS hit analogs
The K$_D$ of nine similarly structured fragment compounds were analyzed to generate this map.

Table 1

X-ray crystallography statistics for the refinement of 4YIW.

4YIW	
Data collection	
Space group	P2(1) (No. 4)
Cell constants (a, b, c, β)	50.18Å 81.68Å 104.53Å 100.29°
Resolution (Å)	19.72 (2.45) Å
Total No. of reflections	211917
No. of averaged reflections (unique reflections)	32367
Redundancy	6.5
R_{merge} (%)	14.0 (99.1)[†]
$<I/\sigma(I)>$	5.84 (1.08)[†]
Completeness (%)	71.0 (99.6)[†]
Refinement	
Resolution range (Å)	19.72-2.45
No. of reflections	28978
No. of reflections in test set	1521
Completeness (%)	99.33
R_{cryst} (%)	20.6
R_{free} (%)	26.5
Wilson B factor (Å^2)	36.9
Mean B factor	42.0
No. of protein molecules in asymmetric unit	2
R.m.s.d.s from ideal geometry	
Bond lengths (Å)	0.006
Bond angles (°)	1.023
Ramachandran plot	
Favoured (%)	93.85
Allowed (%)	5.56
Disallowed (%)	0.59
No. of solvent molecules	310
Ligand	Zn
	NCD
Mean B factor NCD	67.9
Mean B factor H_2O	34.1

[†]Highest resolution shell shown in parentheses

Table 2

Comparison of kinetic values of wild-type and mutants of *B. anthracis* DHOases.

Enzyme	Substrate	K_M (μM)	k_{cat} (s⁻¹)	K_{cat}/K_M (M⁻¹s⁻¹)
WT-DHOase	Ca-asp	112 ± 24	2.1 ± 0.1	1.9×10^4
WT-DHOase	DHO	114 ± 16	1.9 ± 0.1	1.7×10^4
R63A-DHOase	Ca-asp	na	na	na
R63A-DHOase	DHO	na	na	na
N93A-DHOase	Ca-asp	1183 ± 251	1.4 ± 0.1	1.2×10^3
N93A-DHOase	DHO	na	na	na
D304A-DHOase	Ca-asp	na	na	na
D304A-DHOase	DHO	na	na	na

na : no activity (not measurable)
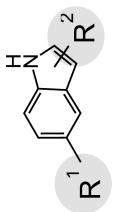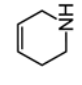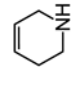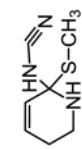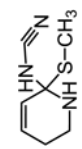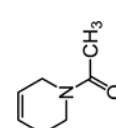
Table 3

Preliminary Structure-Activity Relationship (SAR) of HTS hit analogs.

Compound	MW	R^1	R^2	K$_D$^{a} (μM)	K$_D$ (μM) with 1 mM Ca-asp
6	308.8	-OCH$_3$		380 ± 1	314 ± 34
6a	202.3	-OCH$_3$		588 ± 38	675 ± 12
6b	186.3	-CH$_3$		NB^b	NB^b
6c	176.2	-OCH$_3$	-2-CH$_2$NH$_2$	NB^b	NT^c
7	276.3	-F		67 ± 7	>1 mM
7a	288.4	-OCH$_3$		119 ± 13	144 ± 69
8	244.3	-OCH$_3$		205 ± 8	215 ± 2

^{a}K$_D$: Equilibrium dissociation constant determined by SPR; the standard deviation are from three independent experiments.

^{b}NB: Non-specific binding pattern

^{c}: NT: Not tested